Research Article

Synchrotron Imaging of Ovaries *Ex Vivo*

Upekha Basnayaka[1], Dean Chapman[2], Gregg Adams[3], Tomasz Wysokinski[4], George Belev[4], Rani Kanthan[5], Rajni Chibbar[5], Robert Lewis[4], Naoto Yagi[6], Kentaro Uesugi[6], Masato Hoshino[6] and Angela Baerwald[1]*

[1]*Department of Obstetrics, Gynecology and Reproductive Sciences, College of Medicine, University of Saskatchewan, Saskatchewan, Canada*
[2]*Department of Anatomy and Cell Biology, College of Medicine, University of Saskatchewan, Saskatchewan, Canada*
[3]*Department of Veterinary Biomedical Sciences, Western College of Veterinary Medicine, University of Saskatchewan, Saskatchewan, Canada*
[4]*Canadian Light Source, Saskatchewan, Canada*
[5]*Department of Pathology, College of Medicine, University of Saskatchewan, Saskatchewan, Canada*
[6]*Japan Synchrotron Radiation Research Institute, SPring-8/JASRI, 1 Hyogo Prefecture, Japan*

Abstract

Background: Conventional 2-dimensional ultrasonography is limited in its ability to detect ovarian microanatomy. The objective of this study was to determine if biomedical synchrotron techniques would be effective for imaging ovarian microanatomy, including ovarian follicles, corpora lutea, and the oocyte.

Methods: A prospective, observational study was conducted at the Canadian Light Source to compare ovarian imaging *ex vivo* using propagation-based computed tomography (PB-CT) synchrotron imaging, ultrasonography, and histology. Bovine (n=4) and human (n=4) ovaries were imaged fresh or formalin-fixed. The effectiveness of Talbot grating interferometry computed tomography (TGI-CT) synchrotron imaging to image preserved bovine (n=1) and human (n=1) ovaries was evaluated at the SPring-8 synchrotron, Japan.

Results: All antral follicles ≥ 2 mm and corpora lutea detected with ultrasonography were identified with PB-CT. Mean follicle and luteal diameters did not differ among PB-CT, ultrasonography, and histology. The smallest follicle detected was superior with PB-CT (0.9 ± 0.4 mm) than ultrasonography (2.2 ± 0.2 mm, P<0.05). PB-CT, but not ultrasonography, allowed the detection of follicle wall cell layers (P<0.05). TGI-CT provided greater contrast for evaluating follicles, corpora lutea, and vasculature than PB-CT and ultrasonography. High contrast spherical structures resembling cumulus oocyte complexes were detected with PB-CT and TGI-CT; oocytes were only detected with TGI-CT.

Conclusion: PB-CT was as effective as ultrasonography for measuring follicle and luteal diameters and superior to ultrasonography for visualizing follicles <2 mm, follicle wall cell layers, and cumulus oocyte complexes. TGI-CT appears to provide the greatest resolution for imaging ovarian anatomy compared to ultrasonography and PB-CT. Phase contrast CT Synchrotron can be used as a model for developing high resolution tools for imaging human ovaries.

Keywords: Ovary; Oocyte; Synchrotron; Phase contrast computed tomography

Introduction

Non-invasive imaging technologies are essential for understanding the structural and functional properties of reproductive tissues. Currently, the most commonly used method for evaluating the ovaries is ultrasonography because it is non-invasive, safe, and portable [1]. Obstetrical and gynaecologic applications of ultrasonography include, but are not limited to, monitoring ovarian and uterine function during the menstrual cycle (i.e., follicular, luteal, and endometrial development; ovulation), assessment of embryonic, foetal, and placental development, and the diagnosis and treatment of infertility and pregnancy disorders [2-4].

Ultrasonography has profoundly improved our ability to monitor reproductive function and early development *in vivo*. However, the detection of ovarian microanatomy (i.e., structures approximately <2 mm, such as early developing follicles, cell layers of the follicle wall, and oocytes) are not currently possible using conventional 2-dimensional ultrasonography [5]. In addition, the resolution of ultrasonographic imaging is restricted by penetration depth as well as artefacts caused by intestinal activity and gas [6]. The development of novel high-resolution imaging technologies may increase our understanding of the physiologic mechanisms underlying folliculogenesis, luteal development, oogenesis, and ovulation, and thereby provide insight into female reproductive pathophysiology.

Synchrotron techniques are emerging as a high resolution tool to image normal and pathological biological tissues. Synchrotrons are considered high power light sources. During synchrotron imaging, electrons are accelerated to create a high-energy light beam. Synchrotron imaging can be conducted with lower radiation exposure compared to conventional X-ray methods due to the selection of a photon beam with a narrow energy range [7-11]. The biomedical applications of synchrotron imaging techniques were initially investigated in animal and human tissue samples or whole animals post-mortem. Clinical studies have been further conducted in women to image the breast [12] and scalp [13], and in men to image the hand [14].

Phase-contrast synchrotron imaging utilizes both the refraction and absorption properties of objects to provide images of greater contrast resolution compared to conventional X-ray imaging. As the synchrotron beam traverses an object, the X-rays are refracted and

absorbed. The amount of refraction and absorption depends upon the thickness and density of the object [15-17]. Contrast, produced by the differences in thickness and density, is detected and projected onto an image. Phase-contrast imaging is about 1000 times more powerful for detecting subtle density changes in soft tissues compared to conventional radiography [10,17-20].

Propagation-based imaging (PBI) and Talbot grating interferometry (TGI) imaging are 2 different synchrotron applications that utilize phase-contrast techniques. With each technique, the sample is placed in-line with the incoming X-ray beam. The X-rays that pass through the sample are captured by a detector, which converts the X-rays into visible light [20]. The phase contrast techniques mentioned above can be combined with computed tomography (CT) by rotating the sample and obtaining 2-dimensional slices for each projection [21]. PBI techniques have been used to examine mouse and rabbit lungs [15], as well as the human kidney, prostate [22], and knee [23].

In comparison, TGI uses two gratings to measure the refraction-induced lateral displacement caused by wave interference [18,24,25]. The first grating (i.e., phase grating) is placed behind the sample to create X-ray interference and the second grating (i.e., absorption grating) is placed in front of the detector to generate Moiré fringes [26]. TGI is useful for imaging weakly-absorbing soft tissues; however, it is more difficult to implement than other phase-contrast techniques [9]. TGI synchrotron methods have previously been used to image the mouse heart [26], mouse fetus [27], mouse knee joint [28], rat brain [25,28], rat spinal cord [29], human coronary atherosclerotic plaques [30], and human breast [31].

The objective of this study was to determine the effectiveness of PB-CT and TGI-CT for imaging bovine and human ovaries *ex vivo*. We hypothesized that PB-CT and TGI-CT would provide greater contrast resolution for imaging ovarian structures (i.e., antral follicles, cumulus oocyte complexes, and corpora lutea) compared to conventional 2-dimensional diagnostic ultrasonography.

Materials and Methods

Sample preparation

Phase 1 of this research (i.e., proof of principle study) involved imaging bovine ovaries *ex vivo*. Fresh bovine ovaries (n=4) were collected from local abattoirs in Saskatchewan, Canada. The ovarian artery was flushed with saline within 30 minutes of collection. Samples were imaged fresh without contrast (n=1), fresh with an injection of 5–8 mL of iodine-based contrast agent (Ioversol, Optiray240, St. Louis, Missouri, United States of America) into the ovarian artery (n=2), or after preservation in 10% formalin with ovarian artery contrast (n=1).

The second phase of the research involved imaging human ovaries *ex vivo*. Formalin-fixed human ovarian tissue sections (n=2) were obtained from the Department of Pathology at the Royal University Hospital, Saskatoon, Saskatchewan. In addition, fresh unfixed human ovaries (n=2) were obtained in the operating room from women undergoing bilateral laparoscopic oophorectomy (mean age=50.5 years; range=49-52 years).

Ethical approval for conducting the study was obtained from the Animal Care Committee and the Biomedical Research Ethics Board at the University of Saskatchewan (February, 2011), as well as the Strategic Health Information and Planning Services Unit of the Saskatoon Health Region (June, 2011). Research procedures were conducted in accordance with the Tri-Council Policy Statement on the Ethical Conduct for Research Involving Humans, and the Canadian Council on Animal Care. All human participants provided informed consent before initiating study procedures.

Imaging

Propagation-based computed tomography (PB-CT): Ovaries/ovarian tissues were transported in saline at room temperature to the Canadian Light Source (CLS) for imaging using the BioMedical Imaging and Therapy beamline (05B1-1). Samples were placed in a cylindrical plastic container filled with normal saline and kept at room temperature during imaging. Air bubbles were manually removed from the container prior to imaging. The sample was placed on a stage 27 m from the light source. A detector with a charge-coupled device camera (Appendix A) was placed 125 cm downstream from the sample. Ovaries were scanned from top to bottom for a total of 3–4 image slices of 5 mm each. A total of 1800 projection images, each with a pixel size of 18.8 μm, were obtained for each slice. The total imaging time for a 5 mm-slice of the ovary (26 mm field of view) took approximately 90 minutes. The PBI synchrotron equipment set up is shown in Appendix B.

PB-CT images were reconstructed using SyrmepTomoProject software (Appendix A). File conversions and editing of images were conducted using ImageJ, HCImage, and Avizo Standard (Appendix A). Ring artefacts that were observed in the images were removed using a customized software program [32,33].

Talbot grating interferometry computed tomography (TGI-CT): TGI-CT imaging was conducted at the SPring-8 synchrotron facility (BL20B2 beamline) in Japan. A preserved bovine ovary (n=1) and a preserved human ovarian tissue section (n=1) were imaged. The samples were embedded in agarose gel and imaged with an X-ray energy of 25 keV and a pixel size of 13.3 μm. Images were obtained using a detector with an attached camera (Appendix A). The scanning time was approximately 150 minutes for whole ovaries and 90 minutes for tissue sections. CT scans were conducted by obtaining 900 projections as the sample stage was rotated 180°. A total of 5 images were obtained for each projection by shifting the absorption grating. Specific regions of interest identified in the ovaries during PB-CT were marked with indelible ink for continued TGI-CT imaging. The TGI-CT images were reconstructed using a customized software program (SPring-8, Japan). The TGI synchrotron equipment set-up is illustrated in Appendix B.

Ultrasonography: All ovaries were imaged with 2-dimensional ultrasonography using a portable ultrasonographic system (Appendix A). Ovaries were imaged in a saline bath with the following configurations: depth of 6 cm; overall gain of 52%; single focal zone at a depth of 3 cm. Ultrasonographic images were evaluated using Sante DICOM Editor and ImageJ (Appendix A).

Histology: Upon completion of synchrotron and ultrasonographic imaging, samples were placed in 10% formalin. The specific areas of interest in the ovary, previously marked with indelible ink, were cut in 3 mm slices and mounted in paraffin blocks. The blocks were serially sectioned at a thickness of 5 μm using a microtome, and every fourth section was selected for hematoxylin and eosin staining. Digital images of the histological slides were obtained using a digital camera (Appendix A). Histologic images were edited using ViewNX (Appendix A).

Evaluations

Visual observations/qualitative assessments: Qualitative assessments were made for all samples imaged sequentially with PB-CT, TGI-CT, ultrasonography, and histology. The ability to detect ovarian anatomy of interest (i.e., follicles, corpora lutea, and cumulus oocyte

complexes) using each imaging technique was tabulated and compared. Ovarian follicles were labelled as either healthy or atretic, based on histologic evaluations [34].

Quantitative assessments: Quantitative analyses were conducted for correspondent PB-CT, ultrasonographic, and histologic images. The mean diameter of all antral follicles ≥ 2 mm and all corpora lutea were calculated as the average of the length and width in the transverse plane. The thickness of the follicle wall was measured in replicates at the 2 o'clock, 4 o'clock, 8 o'clock, and 10 o'clock positions and then averaged. The smallest follicle detected was recorded using PB-CT, ultrasonography, and histology [35]. The orientation and magnification of images were standardized for each technique. The mean follicle diameter, mean luteal diameter, and the smallest antral follicle detected were compared among PB-CT, ultrasonography, and histology using One-way analysis of variance with Tukey's post-hoc tests (SPSS Statistics, v20.0, Chicago, Illinois, United States of America). No differences were observed in mean follicle diameter or mean follicle wall measurements between healthy versus atretic follicles; therefore, data were combined.

Results

Propagation-based computed tomography

Corresponding gross, ultrasonographic, PB-CT, and histologic images of a fresh bovine ovary and a formalin-fixed human ovarian tissue segment are shown in Figure 1. All antral follicles ≥ 2 mm detected with ultrasonography were also detected with PB-CT. Antral follicles were identified ultrasonographically as dark, anechoic, circular structures. Antral follicles in the PB-CT images were visualized as circular structures with a more clearly visualized wall; less contrast was observed between the follicle antrum and ovarian stroma with PB-CT versus ultrasonography (Figures 1e and 1f). The granulosa and thecal layers comprising the follicular wall were distinguishable in PB-CT images, but not ultrasonographic images (Figure 1).

All corpora lutea detected with ultrasonography were also visualized with PB-CT. The developing corpus luteum was visualized ultrasonographically as an irregularly circumscribed structure of mixed echotexture with or without a hypo-echoic (i.e., dark) fluid-filled cavity (Figure 1d). In the PB-CT image, the central cavity of the
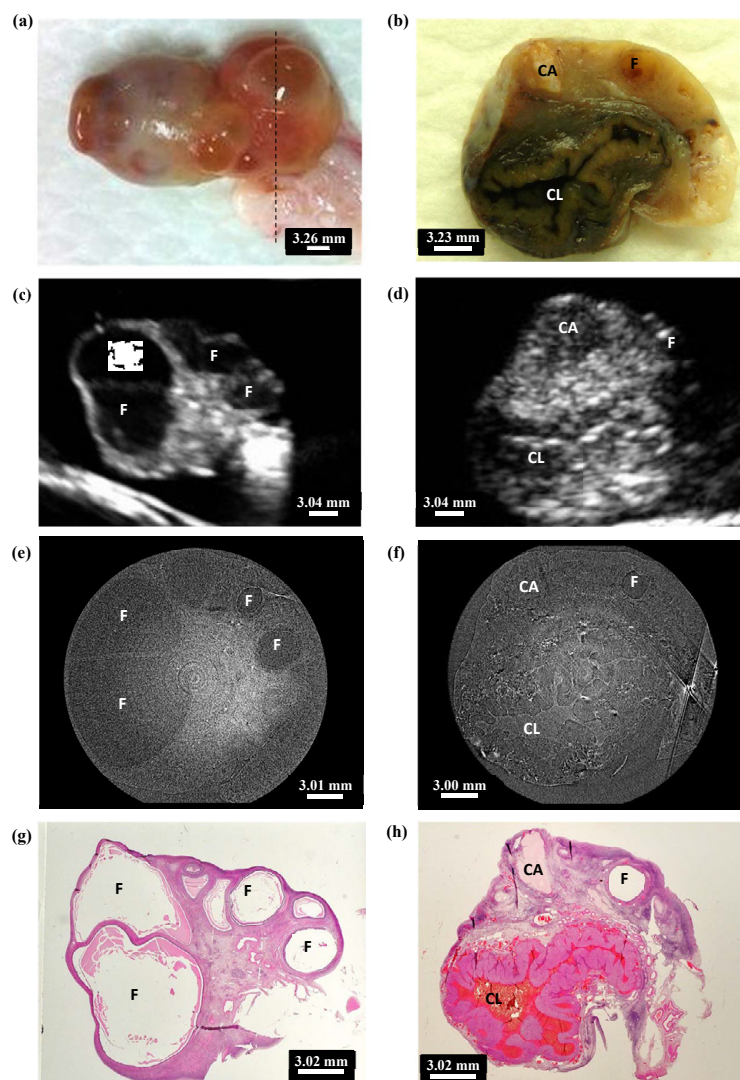
Figure 1: Corresponding projections taken by gross, ultrasonographic, propagation-based computed tomography, and histologic imaging of a fresh bovine ovary (a, c, e, g, respectively) and a hemi-sected formalin-fixed human ovary (b, d, f, h, respectively). Follicles (F), corpus luteum (CL), and corpus albicans (CA) are depicted. The dashed line on the gross image (a) indicates the plane of sectioning.

corpus luteum exhibited greater contrast resolution compared to the luteal tissue (Figure 1f). Furthermore, the borders of the luteal cavity were more clearly visualized in the PB-CT image compared to the ultrasonographic image (Figure 1d). Luteal tissue in the PB-CT images exhibited lower contrast resolution compared to antral follicles (Figure 1f). The contrast resolution of corpora lutea without a fluid-filled cavity was similar to that of the ovarian stroma in the PB-CT images. Therefore, corpora lutea without a fluid-filled cavity were less clearly visualized using PB-CT compared to ultrasonography.

The mean diameters of individual follicles and corpora lutea in both bovine and human ovaries were not different among PB-CT, ultrasonography, and histologic images (Table 1). PB-CT and histology were more sensitive than ultrasonography for detecting small antral follicles in bovine ovaries (Table 2, P=0.04). The mean follicle wall thickness in bovine and human ovaries was smaller using both PB-CT and histology compared to ultrasonography (Table 3, P<0.0001).

Ring artefacts were observed as dark and bright concentric circles in the reconstructed PB-CT images (Figures 1e and 1f). Removal of ring artefacts resulted in a reduction in the overall contrast of PB-CT images; therefore, ring artefacts were not removed. Preservation of the ovaries caused slight shrinkage of the tissues; however, no differences in image quality were observed.

Talbot grating interferometry computed tomography

Gross morphology, ultrasonography, PB-CT, and TGI-CT images of a bovine ovary (Figures 2a, 2c, 2e and 2g) and human ovarian tissue segment (Figures 2b, 2d, 2f and 2h) were compared. Overall, the image

Sample	n	PB-CT (mm)	Ultrasonography (mm)	Histology (mm)	P-value
Bovine Ovaries: Follicle Diameter					
Preserved- with contrast	11	4.2 ± 0.8	4.7 ± 0.8	3.8 ± 0.7	0.72
Fresh - with contrast	19	4.7 ± 0.7	5.3 ± 0.6	4.0 ± 0.6	0.33
Fresh - no contrast	1	4.6	5.6	5.0	-
Human Ovaries: Follicle Diameter					
Preserved- no contrast	5	4.6 ± 0.5	4.0 ± 0.43	3.7 ± 0.4	0.38
Fresh - no contrast	4	6.1 ± 2.5	5.0 ± 1.8	4.6 ± 1.6	0.79
Human Ovaries: Luteal Diameter					
Preserved - no contrast	2	8.9 ± 5.4	8.1 ± 3.8	7.0 ± 3.9	0.65
Fresh - no contrast	2	3.4 ± 0.5	4.5 ± 0.3	3.6 ± 0.3	0.16

Mean bovine luteal diameter was not calculated due to limited sample size.
n=number of follicles/corpora lutea
PB-CT=Propagation-Based Computed Tomography

Table 1: Diameter (mean ± standard error) of individual follicles and corpora lutea in bovine and human ovaries.
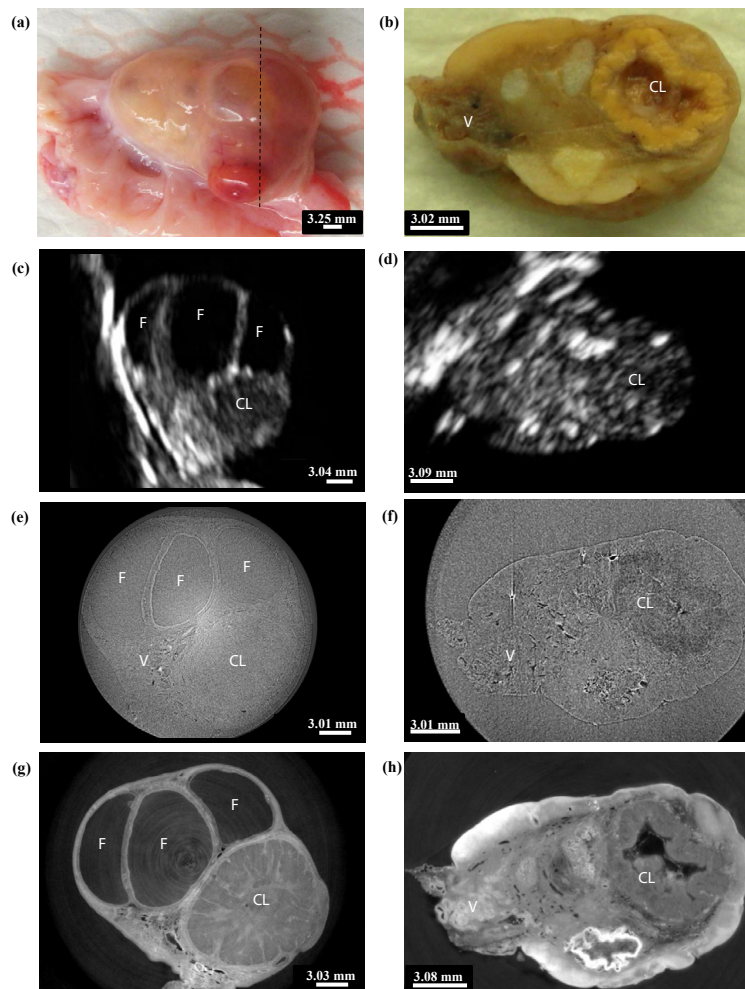
Figure 2: Images of a preserved bovine ovary (a, c, e, g) and a formalin-fixed human ovarian tissue segment (b, d, f, h) obtained using the 4 different imaging techniques. Correspondent gross (a, b), ultrasonographic (c, d), propagation-based computed tomography (e, f), and Talbot grating interferometry computed tomography (g, h) images are shown. Follicles (F), corpus luteum (CL), and vasculature (V) are indicated. The dashed line on the gross image (a) indicates the plane of sectioning.

Sample Condition	n	PB-CT (mm)	Ultrasonography (mm)	Histology (mm)
Bovine ovaries	3	0.9 ± 0.4[a]	2.2 ± 0.2[b]	0.2 ± 0.1[a]
Human ovaries	4	1.2 ± 0.7[a]	2.7 ± 0.4[a]	0.9 ± 0.6[a]

[a,b] Within rows, values with different superscripts are different (P < 0.05)
n=number of ovaries
PB-CT=Propagation-based Computed Tomography

Table 2: Diameter (mean ± standard error) of the smallest follicle detected in bovine and human ovaries using propagation-based computed tomography, ultrasonography, and histology.

Sample	n	PB-CT (mm)	Ultrasonography (mm)	Histology (mm)
Bovine Ovaries				
Preserved - with contrast	10	0.15 ± 0.01[a]	0.31 ± 0.01[b]	0.15 ± 0.01[a]
Fresh - with contrast	17	0.16 ± 0.01[a]	0.27 ± 0.01[b]	0.14 ± 0.01[a]
Fresh - no contrast	1	0.31	0.14	0.14
Human Ovaries				
Preserved - no contrast	5	0.16 ± 0.01[a]	0.28 ± 0.02[b]	0.10 ± 0.01[a]
Fresh - no contrast	2	0.17 ± 0.02[a]	0.30 ± 0.03[b]	0.12 ± 0.01[a]

[a,b] Within rows, values with different superscripts are different (P < 0.05)
n=number of follicles
PB-CT=Propagation-Based Computed Tomography

Table 3: Follicle wall thickness (mean ± standard error) in bovine and human ovaries obtained using propagation-based computed tomography, ultrasonography, and histology.

contrast and resolution were markedly superior using TGI-CT versus PB-CT and ultrasonography. Follicles and corpora lutea were more clearly visualized in TGI-CT images. The theca and granulosa cell layers comprising the follicle wall were visualized with both PB-CT (Figure 2e) and TGI-CT (Figure 2g) but not ultrasonography (Figure 2c); however, they were most clearly visualized with TGI-CT. Irregular and invaginated walls of corpora lutea were better distinguished with TGI-CT (Figures 2g and 2h) compared to PB-CT (Figures 2e and 2f) and ultrasonography (Figures 2c and 2d). Ovarian vasculature was most clearly detected with TGI-CT (Figures 2g and 2h), less clearly detected with PB-CT (Figures 2e and 2f), and not detected with ultrasonography (Figures 2c and 2d).

High contrast spherical structures <0.60 mm, protruding into the follicle antrum from the wall, were identified in bovine ovaries using PB-CT (n=9 follicles, 3 ovaries) and TGI-CT (n=7 follicles, 1 ovary) imaging. The location, size, and shape of these protrusions were consistent with cumulus-oocyte complexes. The image contrast resolution of the apparent cumulus-oocyte complexes was superior with TGI-CT compared to PB-CT, such that the oocyte within the complex of cumulus granulosa cells could be observed in the TGI-CT images. An example of a cumulus oocyte complex identified using both PB-CT and TGI-CT imaging is shown in Figure 3 a and b.

Discussion

In this pilot study, we examined the effectiveness of PB-CT and TGI-CT synchrotron techniques for imaging ovarian microanatomy, including antral follicles, corpora lutea and cumulus oocyte complexes. Encouraging results obtained from the first phase of our research using the bovine species were applied to the continued evaluation of PB-CT and TGI-CT synchrotron imaging in humans. Overall, we concluded that PB-CT and TGI-CT imaging techniques provided greater contrast resolution for visualizing ovarian micoanatomy *ex vivo* compared to conventional 2-dimensional ultrasonography. PB-CT was superior to ultrasonography for detecting small antral follicles <2 mm, cell layers of the follicle wall, and cumulus oocyte complexes, and equivalent to ultrasonography for measuring follicle and luteal diameters. We obtained preliminary data to demonstrate that TGI-CT provided the greatest contrast for visualizing ovarian microanatomy compared to both PB-CT and ultrasonography *ex vivo*. Therefore, our hypotheses were supported.

Follicles are the structural and functional units of the ovary. Therefore, the ability to evaluate follicular morphology is crucial for understanding normal and abnormal female reproductive function. The multiple scans obtained with CT synchrotron techniques enabled us to evaluate the ovary in serial cross sections and identify individual antral follicles of various sizes. PB-CT imaging was as effective as ultrasonography for measuring antral follicles ≥ 2 mm in bovine and human ovaries. However, the detection of small antral follicles <2 mm was superior with PB-CT compared to ultrasonography. These findings are clinically relevant because there are currently no non-invasive imaging tools that allow the detection of small antral follicles. Greater information about how early (i.e., pre-antral and early antral) follicles develop and regress is essential for understanding changes in ovarian function associated with age and/or infertility [36,37]. Similarly, the wall of bovine and human follicles was more clearly visualized and more accurately measured using PB-CT versus ultrasonography when both methods were compared with histology. The ability to detect changes in the microanatomy of the follicle wall has clinical relevance for detecting ovulation as well as early stage ovarian malignancies in women. Compared to both ultrasonography and PB-CT, TGI-CT synchrotron imaging provided the greatest contrast resolution for imaging antral follicles.

Microanatomy detected within the TGI-CT images better resembled histology compared to PB-CT. Circular structures were detected within the follicular antrum using PB-CT. We interpreted the spherical structures to be cumulus oocyte complexes due to their size, location and morphology, as previously characterized using ultrasound biomicroscopy [35,36]. Smaller circular structures within the cumulus oocyte complexes were further identified in the TGI-CT images, and
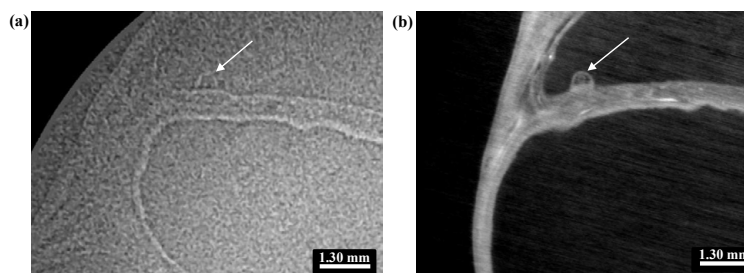
Figure 3: Images of a bovine ovary obtained using propagation-based computed tomography (a) and Talbot grating interferometry computed tomography (b) synchrotron techniques. Arrows indicate the cumulus-oocyte-complex attached to the wall of the follicle.

were thought to represent the oocyte, itself. To our knowledge, this is the first documentation of detecting human oocytes within the cumulus oocyte complex using imaging techniques. Unfortunately, oocytes were not visualized in the slices that were chosen for histologic evaluation. This finding is due to the impracticality in analysing all histologic sections of each ovary. Furthermore, very few follicles were present within the human ovaries, as most women undergoing surgical removal of the ovaries were post-menopausal and had a reduced ovarian reserve [38]. We believe that our findings provide rationale for continued research to image human cumulus oocyte complexes using PB-CT and TGI-CT *in vivo* in women of reproductive-age. Detection of bovine oocytes *ex vivo* in the present study is consistent with previous research in which synchrotron-based Fourier transform-infrared microspectroscopy and X-ray fluorescence microscopy were used to evaluate the composition, biochemistry, and elemental mapping of mouse and frog oocytes *ex vivo* [37,39]. The ability to visualize the oocyte *in vivo* is not possible at present, but would be a major advancement in female reproductive imaging for both conceptive and contraceptive purposes.

Accurate identification of the corpus luteum is important for assessing ovulation and fertility potential in women undergoing assisted reproduction [40]. PB-CT was as effective as ultrasonography for measuring luteal diameter and differentiating cystic corpora lutea from follicles. However, non-cystic corpora lutea were not well visualized using PB-CT. Furthermore, PB-CT and ultrasonography were capable of detecting only some of the corpora lutea that were visualized histologically. In comparison, TGI-CT enabled the detection of all luteal structures regardless of a central cystic cavity. The resolution of the luteal stroma and antra was superior with TGI-CT versus PB-CT and ultrasonography. We attribute the superiority of TGI-CT for luteal imaging to the fine contrast details produced by the distribution of X-rays through the crystal gratings.

One of the limitations of this pilot study was the time required for synchrotron imaging. The total length of time required for synchrotron sample set-up, beamline preparation, and imaging of a whole ovary (approximately 3 cm × 2 cm × 1 cm) was approximately 8 hours, which limited the number of samples that we could image. Imaging a greater number of specimens and creating a greater number of slices/specimen would have increased the probability of detecting human oocytes in correspondent synchrotron and histologic images. Another limitation of our study was the presence of ring artefacts in the PB-CT images, which were attributed to imperfect detector elements [41]. When we attempted to remove these artefacts, we observed an overall reduction in image quality. We propose that continued research using a different detector may improve the quality of PB-CT images. Moreover, it is possible that a combination of two or more synchrotron-based phase-contrast techniques would be useful. In the present study, quantitative measurements from synchrotron, ultrasound, and histologic images were made by a single investigator. We recognize that ultrasonographic imaging is an operator dependant technique. Thus, assessment of blinded images by more than one investigator may have strengthened our study design.

At present, synchrotron imaging of human reproductive tissues is experimental. The radiation dose of conventional CT imaging is typically 1 mGy-15 mGy per CT scan (corresponding to 1μGy-10 μGy per projection), providing a resolution of 0.5 mm voxel size. By comparison, the radiation dose used in the present study was estimated to be 10 mGy-40 mGy per projection, providing a much greater resolution of 0.014 mm-0.019 mm in voxel size, necessary for detecting ovarian microanatomy. The radiation dose used in the present study is not acceptable for clinical use. In the clinical setting, a suitable energy and safe radiation exposure time will be required without compromising the resolution and quality of the images. In addition to radiation dose, the scanning time of 1.5 hours to 2.5 hours in the present study is not practical for clinical use. The cost of conducting synchrotron imaging in the clinical setting is currently unknown, but is an additional consideration. Overall, the results of this pilot study are an important first step for continued research to validate safe, effective, and practical imaging techniques for the clinical evaluation of human reproductive tissues *in vivo*. The next phase of this research is to optimize phase contrast CT synchrotron techniques that will provide high resolution imaging of targeted areas of interest, allowing a reduction in radiation exposure and a shortened timeframe. Research is ongoing at the Canadian Light Source to further develop synchrotron biomedical imaging, with the long-term goal of clinical diagnostic use. Continued developments in high-resolution *in vivo* synchrotron imaging may enhance our understanding of ovarian physiology and pathology, which may in turn provide insight into improving the diagnosis and clinical management of reproductive dysfunction in women [42]. Furthermore, the development of novel synchrotron methods for imaging ovaries may be applied to the detection and characterization of other soft tissues, such as the prostate and breast.

In summary, PB-CT was as effective as ultrasonography for measuring follicle and luteal diameter and superior to ultrasonography for visualizing follicles <2 mm, cell layers of the follicle wall and cumulus oocyte complexes. However, TGI-CT appeared to provide the greatest resolution for imaging ovarian anatomy compared to both ultrasonography and PB-CT. Continued research is required to further optimize phase contrast synchrotron imaging with the goal of providing a safe and practical means for clinically evaluating human ovarian anatomy, physiology, and pathophysiology.

Acknowledgement

References

1. Mihu D, Mihu CM (2011) Ultrasonography of the uterus and ovaries. Med Ultrason 13: 249-252.

2. Adams GP, Pierson RA (1995) Bovine Model for Study of Ovarian Follicular Dynamics in Humans. Therio 43: 113-120.

3. Bomsel-Helmreich O (1985) Ultrasound and the preovulatory human follicle. Oxf Rev Reprod Biol 7: 1-72.

4. Saba L, Guerriero S, Sulcis R, Virgilio B, Melis G, et al. (2009) Mature and immature ovarian teratomas: CT, US and MR imaging characteristics. Eur J Radiol 72: 454-463.

5. Baerwald AR, Adams GP, Pierson RA (2003) Characterization of ovarian follicular wave dynamics in women. Biol Reprod 69: 1023-1031.

6. Harris RA, Follett DH, Halliwell M, Wells PN (1991) Ultimate limits in ultrasonic imaging resolution. Ultrasound Med Biol 17: 547-558.

7. Arfelli F (2000) Synchrotron light and imaging systems for medical radiology. Nucl Instrum Meth A 454: 11-25.

8. Kocsis M, Snigirev A (2004) Imaging using synchrotron radiation. Nucl Instrum Meth A 525: 79-84.

9. Margaritondo G (2002) Smart-tourist guide to a synchrotron light facility. In: Margaritondo G (eds), Elements of synchrotron light for biology, chemistry and medical research. Oxford University Press, Oxford.

10. Suortti P, Thomlinson W (2003) Medical applications of synchrotron radiation. Phys Med Biol 48: R1-35.

11. Westneat MW, Socha JJ, Lee WK (2008) Advances in biological structure, function, and physiology using synchrotron X-ray imaging. Annu Rev Physiol 70: 119-142.

12. Dreossi D, Abrami A, Arfelli F, Bregant P, Casarin K, et al. (2008) The mammography project at the SYRMEP beamline. Eur J Radiol 68: S58-62.

13. Han SM, Chikawa JI, Jeon JK, Hwang MY, Lim J, et al. (2015) Synchrotron nanoscopy imaging study of scalp hair in breast cancer patients and healthy individuals: Difference in medulla loss and cortical membrane enhancements. Microsc Res Tech 79: 23-30.

14. Momose A, Yashiro W, Kido K, Kiyohara J, Makifuchi C, et al. (2014) X-ray phase imaging: from synchrotron to hospital. Philos Trans A Math Phys Eng Sci 372: 20130023.

15. Kitchen MJ, Lewis RA, Yagi N, Uesugi K, Paganin D, et al. (2005) Phase contrast X-ray imaging of mice and rabbit lungs: a comparative study. Br J Radiol 78: 1018-1027.

16. Lewis R (2005) Medical applications of synchrotron radiation in Australia. Nucl Instrum Meth A 548: 23-29.

17. Zhou SA, Brahme A (2008) Development of phase-contrast X-ray imaging techniques and potential medical applications. Phys Med 24: 129-148.

18. Momose A, Washiro W, Takeda Y, Suzuki Y, Hattori T (2006) Phase-imaging with an x-ray talbot interferometer. JCPDS-International Centre for Diffraction Data: 21-30.

19. Snigirev A, Snigirev I, Kohn V, Kuznetsov S, Schelokov I (1995) On the possibilities of x-ray phase contrast microimaging by coherent high-energy synchrotron radiation. Rev Sci Instrum 66: 5486-5492.

20. Socha JJ, Westneat MW, Harrison JF, Waters JS, Lee WK (2007) Real-time phase-contrast x-ray imaging: a new technique for the study of animal form and function. BMC Biol 5: 6.

21. Wu X, Liu H, Yan A (2008) Phase-contrast X-ray tomography: contrast mechanism and roles of phase retrieval. Eur J Radiol 68: S8-12.

22. Yoon CY, Sung DJ, Lee JH, Kim AR, Oh CW, et al. (2007) Imaging of renal and prostate carcinoma with refractive index radiology. Int J Urol 14: 96-103.

23. Horng A, Brun E, Mittone A, Gasilov S, Weber L, et al. (2014) Cartilage and soft tissue imaging using X-rays: propagation-based phase-contrast computed tomography of the human knee in comparison with clinical imaging techniques and histology. Invest Radiol 49: 627-634.

24. Fitzgerald R (2000) Phase-sensitive x-ray imaging. Physics Today 53: 23-26.

25. Pinzer BR, Cacquevel M, Modregger P, McDonald SA, Bensadoun JC, et al. (2012) Imaging brain amyloid deposition using grating-based differential phase contrast tomography. Neuroimage 61: 1336-1346.

26. Weitkamp T, David C, Bunk O, Bruder J, Cloetens P, et al. (2008) X-ray phase radiography and tomography of soft tissue using grating interferometry. Eur J Radiol 68: S13-17.

27. Hoshino M, Uesugi K, Tsukube T, Yagi N (2014) Quantitative and dynamic measurements of biological fresh samples with X-ray phase contrast tomography. J Synchrotron Radiat 21: 1347-1357.

28. Zhu P, Zhang K, Wang Z, Liu Y, Liu X, et al. (2010) Low-dose, simple, and fast grating-based X-ray phase-contrast imaging. Proc Natl Acad Sci U S A 107: 13576-13581.

29. Takashima K, Hoshino M, Uesugi K, Yagi N, Matsuda S, et al. (2015) X-ray phase-contrast computed tomography visualizes the microstructure and degradation profile of implanted biodegradable scaffolds after spinal cord injury. J Synchrotron Radiat 22: 136-142.

30. Winklhofer S, Peter S, Tischler V, Morsbach F, von Werdt M, et al. (2015) Diagnostic Accuracy of Quantitative and Qualitative Phase-Contrast Imaging for the *ex Vivo* Characterization of Human Coronary Atherosclerotic Plaques. Radiology 277: 64-72.

31. Schleede S, Bech M, Grandl S, Sztrókay A, Herzen J, et al. (2014) X-ray phase-contrast tomosynthesis for improved breast tissue discrimination. Eur J Radiol 83: 531-536.

32. Kyriakou Y, Prell D, Kalender WA (2009) Ring artifact correction for high-resolution micro CT. Phys Med Biol 54: N385-391.

33. Wei Z, Wiebe S, Chapman D (2013) Ring artifacts removal from synchrotron CT image slices. J Instrum 8: 1-12.

34. Gougeon A (2004) Dynamics of Human Follicular Growth: Morphologic, Dynamic, and Functional Aspects. In: Leung P, Adashi E (Eds), The Ovary. (2nd Edn), Elsevier Acadmic Press, Amsterdam.

35. Baerwald A, Dauk S, Kanthan R, Singh J (2009) Use of ultrasound biomicroscopy to image human ovaries *in vitro*. Ultrasound Obstet Gynecol 34: 201-207.

36. Pfeifer LF, Siqueira LG, Adams GP, Pierson RA, Singh J (2012) In vivo imaging of cumulus-oocyte-complexes and small ovarian follicles in cattle using ultrasonic biomicroscopy. Anim Reprod Sci 131: 88-94.

37. Wood BR, Chernenko T, Matthäus C, Diem M, Chong C, et al. (2008) Shedding new light on the molecular architecture of oocytes using a combination of synchrotron Fourier transform-infrared and Raman spectroscopic mapping. Anal Chem 80: 9065-9072.

38. Fauser BC (2000) Follicle pool depletion: factors involved and implications. Fertil Steril 74: 629-630.

39. Kim AM, Vogt S, O'Halloran TV, Woodruff TK (2010) Zinc availability regulates exit from meiosis in maturing mammalian oocytes. Nat Chem Biol 6: 674-681.

40. Baerwald AR, Adams GP, Pierson RA (2005) Form and function of the corpus luteum during the human menstrual cycle. Ultrasound Obstet Gynecol 25: 498-507.

41. Munch B, Trtik P, Marone F, Stampanoni M (2009) Stripe and ring artifact removal with combined wavelet--Fourier filtering. Opt Express 17: 8567-8591.

42. Bushnik T, Cook JL, Yuzpe AA, Tough S, Collins J (2012) Estimating the prevalence of infertility in Canada. Hum Reprod 27: 738-746.